Published by
NIGERIAN SOCIETY OF PHYSICAL SCIENCES
Available online @ https://journal.nsps.org.ng/index.php/jnsps

J. Nig. Soc. Phys. Sci. 4 (2022) 497

Journal of the Nigerian Society of Physical Sciences

Geohydraulic characteristics and groundwater vulnerability assessment of tropically weathered and fractured gneissic aquifers using combined georesistivity and geostatistical methods

A. S. Akingboye[a,*]

[a] *Department of Earth Sciences, Adekunle Ajasin University, 001 Akungba-Akoko, Ondo State, Nigeria.*

Abstract

Sustainable groundwater yield in aquifers depends on the protective capacity of the subsurface lithologies and conduit systems. Electrical resistivity tomography (ERT) and its Schlumberger vertical electrical sounding (VES) technique were employed to assess the groundwater yield of aquifer units and their vulnerability to contaminants in Araromi (Akungba-Akoko), southwestern Nigeria. Geohydraulic parameters: aquifer resistivity (ρ_0), hydraulic conductivity (K), transmissivity (T), permeability (Ψ), hydraulic resistance (K_R), and longitudinal conductance (S) were also evaluated. In addition, regression analysis was utilized to establish the empirical relationships between the K and other geohydraulic parameters, with their percentage contributions to posing vulnerability risk. The georesistivity results revealed four distinct layers: topsoil, weathered layer, partially weathered/fractured bedrock unit, and fresh bedrock. The K model regression-assisted analysis showed that the ρ, T, Ψ, and S contributed about 97.8%, 14%, 99.9%, and 11.5%, respectively, to the estimated aquifers' K values for the study area. Except for T and S, the regression results had moderate to strong positive correlations with K; hence, this illuminates the essentiality of K in assessing groundwater potential and vulnerability. The aquifer units have low to moderate groundwater yield based on T values (1.67−17.57 m/day) caused by the generally thin overburden (<4 m). However, the deep-weathered and fractured aquifer units with depths ranging from 39-55 m could supply high groundwater yield for sustainable abstraction. The estimated S values (0.0226−0.1926 mhos) for aquifer protective capacity ratings rated the aquifer units in the area as poor to weak. Based on the estimated low logarithm of K_R (log K_R) values of 0.79−2.25 years, these aquifers have extremely high to moderate aquifer vulnerability index. As a result, prospective wells/boreholes in the study area and settings with similar geohydraulic and vulnerability characteristics should be developed adequately to prevent the infiltration of surface contaminants for potable groundwater abstraction.

DOI:10.46481/jnsps.2022.497

Keywords: Electrical resistivity tomography (ERT), Schlumberger vertical electrical sounding (VES), Geoelectrohydraulic parameters, Regression analysis, Groundwater vulnerability, Gneissic aquifers.

Article History :
Received: 01 December 2021
Received in revised form: 15 July 2022
Accepted for publication: 14 September 2022
Published: 19 November 2022

Communicated by: S. J. Adebiyi

1. Introduction

Globally, the percentage of potable water available to people has declined due to the increasing global population [1, 2, 3]. Sustainable groundwater yield in aquifer zones

*Corresponding author tel. no: +2347032462342
Email address: adedibu.akingboye@aaua.edu.ng (A. S. Akingboye)

depends on the nature of subsurface lithologic units and their water retention capacity, porosities, permeabilities, and water-rock interactions, as well as the hydrodynamics of the aquifer units [3, 4, 5, 6, 7]. The sustainability of groundwater supplies also depends on the quality of the aquifers' yield, which is a function of the protective capacity of the lithologic unit overlying the aquifer zones and their depths. The occurrences of aquifer zones at shallow depths, especially within the crystalline basement terrain, give easy access for the percolation of surface runoffs and pollutants from dumpsites' leachate flows, surface and buried oil tank spillages, dissolved chemicals from mining activities, sewage from sanitation systems, etc., to degrade the groundwater system [8, 9]. In addition, over-stretching of aquifers caused by over-abstraction of groundwater and silt/clay intrusion from improperly cased boreholes degrades groundwater quality [10, 11, 12].

Geoelectrical resistivity profiling and vertical electrical sounding (VES) techniques as well as estimating geohydraulic parameters from resistivity or pumping test datasets have been employed to determine the groundwater potential and vulnerability of aquifer units in several geological terrains [4, 8, 10, 13, 14]. However, the pumping test method is time-consuming and expensive. Hence, it is rarely utilized in geohydraulic evaluation nowadays. The georesistivity methods, on the other hand, are cost-efficient and rapid, and produce quality results with a higher success rate [9, 15]. The georesistivity method provides a good correlation between measured resistivity values and groundwater hydraulic parameters. As a result, the data obtained provide a high-quality estimate of geohydrodynamics and protective capacity ratings of the near-surface lithologic units. These are essential in selecting suitable points for sustainable potable groundwater development [8, 16].

The study area is located in the Araromi area of Akungba-Akoko, southwestern Nigeria. It is situated between Akungba-Akoko Township and Etioro-Akoko and is underlain by complex subsurface geology [3, 7, 17, 18, 19]. The study area has become a choice location for many locals, staff, and students of Adekunle Ajasin University, Akungba-Akoko (AAUA) due to its serenity and prospect of rapid urbanization. Generally, the overburden in the areas is thin, resulting in the failure rates of hand-dug wells and boreholes to meet the growing population. This is caused by low groundwater yield in shallow aquifers, especially during the long dry season period. The groundwater potential of the northern section of the present study area was evaluated using the Schlumberger VES technique by [18]. The authors delineated shallow to deep-weathered/fractured aquifer units responsible for low to moderate groundwater yield. In the same geologic terrain, [3] investigated the near-surface crustal architecture and geohydrodynamics of the Araromi area, Akungba-Akoko using the integrated coplanar loop electromagnetic conductivity method, electrical resistivity tomography (ERT), and Schlumberger VES technique to proffer solutions to the challenges of groundwater availability and the failure of structural engineering foundations in this area. The authors also had similar results to [18], except that high groundwater yield was identified at highly conductive deep fractured zones extending to depths >52 m despite the thin overburden (<4 m). Furthermore, the subsurface geological, hydrogeophysical, and engineering properties and the vulnerability of the southern part (Etioro-Akoko) have been carried out and reported in [7, 17]. These studies indicated that most aquifer units occurred at shallow depths, except for the localized deep-weathered and fractured aquifers.

Despite many previous studies, the vulnerability of the aquifer units in the Araromi area of Akungba-Akoko has not been evaluated. Hence, it has become imperative to expand on the existing knowledge about the vulnerability of the aquifer units to contaminants. The fracture densities and groundwater potential of some identified aquifers can also offer clues on the migration rate of possible contaminants in the study area. Therefore, ERT, VES, and regression analysis were employed to evaluate the groundwater potential and contaminants' vulnerability of aquifer units in the study area. Generally, this study would alleviate the deficiency of groundwater potability in the study area and its environs.

2. Location and Geological Setting of the Study Area

The study area is Araromi in the Akungba-Akoko district of southwestern Nigeria. It falls within latitudes 07°27′02″ N and 07°27′09″ N, and longitudes 005°43′53″ E and 005°44′01″ E in the northern part of Ondo State, Nigeria (Figures 1 and 2). The Nigerian rainforest climatic conditions characterize the area. The area has topographic features consisting of hills, low-lying outcrops, plains, and valleys, between 280 m and 400 m above the mean sea level. The dendritic drainage system follows these topographic features, with trellis drainage patterns in a few places [3, 7].

The study area is parts of the Precambrian Basement Complex of Southwester Nigeria - a prolongation of the reactivated Pan-African mobile belt, which lies east of the West African Craton and northwest of the Congo-Gabon Craton [20, 21, 22, 23, 24], Figure 1a. The Southwestern Basement Complex of Nigeria comprises three major rock suites, namely the Migmatite-Gneiss Complex, the Schist belt, and the Older Granitoid. The Migmatite-Gneiss Complex rocks range in age from Neoproterozoic to Paleoproterozoic and Archean [20, 21, 22]; the Neoproterozoic Schist Belts, consisting of low-grade, younger metasedimentary, and metavolcanic rocks with ages ranging between 690 and 489 Ma [21, 24, 25], and the Pan-African Older Granites, which intruded the two earlier lithologies, have ages ranging between 650 and 580 Ma [25, 26, 27, 28].

The entire Akungba-Akoko is underlain by the Migmatite-Gneiss Complex rocks of southwestern Nigeria, which were intruded by the Pan-African granitoid (Figure 1c). The Migmatite-Gneiss Complex rocks in the area are typically

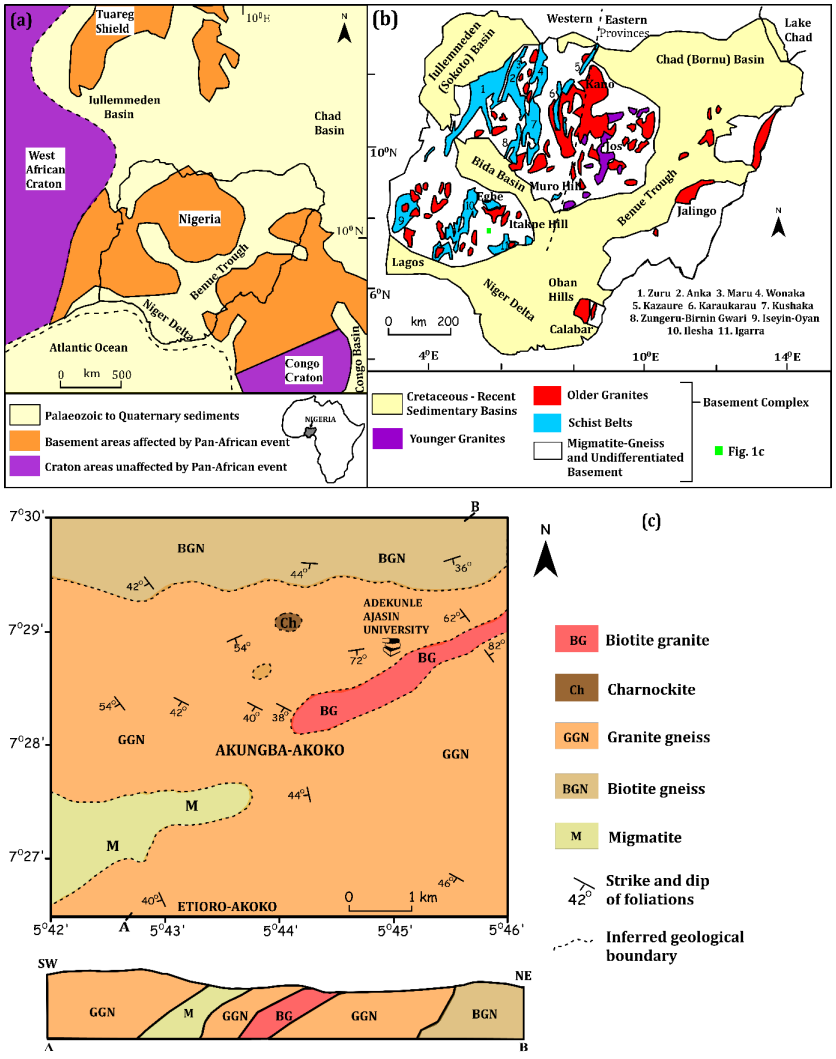

Figure 1: (a) Regional geological map of Nigeria within the Pan-African mobile belt between the West African and Congo Cratons. (b) Detailed geological map of Nigeria, showing the study area (modified after [31]). (c) Geological map of Akungba-Akoko and its surroundings in Ondo State, southwestern Nigeria, modified after [27].

migmatite, granite gneiss, biotite gneiss, and granitoids (charnockite and granite). Granite gneiss is the most abundant rock type in the area, underlying the Araromi part of the area. The granite gneissic rock type has a blastoporphyritic to porphyroblastic fabric and is light grey, medium to coarse-grained, and moderately foliated (light and dark-colored bands). Far to the west, the rock is extensively deformed and migmatized, forming migmatite with an ENE-WSW trend. In addition, intrusions such as quartz veins, pegmatite, aplite, basic dykes, and sills characterized the granite gneisses in the area [3, 21, 27, 29]. The tropical climatic conditions and the metamorphic activities in the Akungba-Akoko Basement Complex terrain have assisted in the weathering and fracturing of the subsurface geology.

The subsurface hydrogeological features of the Araromi area of Akungba-Akoko are similar to those of the surrounding towns, e.g., the Akungba-Akoko town and Etioro-Akoko community [3, 7, 18], as well as some places in the crystalline basement of southwestern Nigeria [9, 30]. The groundwater in the study area occurs in weathered and/or fractured aquifer zones. Groundwater occurrence in these hydrogeologic units is unevenly distributed, just like other Precambrian basement terrains. Generally, the aquifers in the area are characterized by shallow depths with low porosity and permeability. They depend on secondary porosity from deeply weathered and fractured rock units for migrating and storing fluids sufficiently in subsurface strata. It has been reported that the aquifer zones in the study area and surrounding communities have an average depth of about 12 m, exceeding 25 m for deeply weathered and fractured aquifer units [3, 7].

3. Methods

3.1. Field Data Measurements

Six traverses were occupied in the study area to characterize the subsurface lithologies, hydrodynamics, degree of weathering, and fractures, as shown in Figures 2a-b. Traverses

1−3 and 4−6 were established in the NNE-SSW and NW-SE directions, respectively. Traverses 1, 2, and 6 each had a survey profile length of 160 m, but Traverse 3 had a survey profile length of just 100 m due to building obstruction. The survey spread length for Traverse 4 was 150 m, although the ERT profile was terminated at a distance of 145 m from the starting electrode. Figure 2a and b shows that Traverse 5 was 110 m in length. The choice of traverses establishment was based on the availability of adequate spaces for long profiles and places with serious groundwater deficits in the study area.

The ABEM Resistivity Imaging System was used for the ERT field data acquisition, utilizing the dipole-dipole electrode configuration array. The array is sensitive to vertical and lateral subsurface structural variations and low electromagnetic coupling effects [32, 33]. A station interval of 5 m was adopted for the detailed subsurface imaging of the anomalous features of interest for this study. However, the adopted n-level of 5, i.e., ($n = 5$) for dipole-dipole resistivity surveys, could limit probing depths. Nevertheless, the adopted station interval (5 m) was considered suitable for high-resolution near-surface imaging and attenuating surface artifacts arising due to the complex geological conditions of the study area. The Schlumberger VES technique, on the other hand, was carried out at the selected conductive or relatively conductive survey station points to address depth limitations. The generated VES results was used to constrain the ambiguities in the ERT models and to image deep-weathered bodies and the penetrative fractures. Figure 2b depicts the spatial distribution of the investigated VES station points, whereas Figure 2b-c depicts the elevation of the surface topography. The current electrodes AB/2 varied from 60 to 160 m, while the potential electrodes spread MN varied from 0.5 to 15 m. The penetration depth in a homogenous subsurface geologic structure is proportional to the distance between the current electrodes, whereas varying the electrodes distance offers information regarding the subsurface lithologic units [3, 9]. When a remarkable resistivity value $>1000\ \Omega \cdot m$, indicating the fresh bedrock, was attained more than twice at each VES station, the survey was stopped. This is probably an indication of no fracture at deeper depths. However, the barriers encountered due primarily to buildings during the surveys sometimes halted the surveys before the resistivity of the fresh bedrock was recorded.

3.2. Field Data Processing and Modeling

The results from the ERT surveys were processed and inverted using RES2DINV software [32, 34]. The forward modeling and data inversion, utilizing the robust least-squares inversion approach, were used to derive the subsurface resistivity distribution from apparent resistivity measurements. Many previous workers have demonstrated the inversion procedures for the RES2D data inversions, e.g., [3, 11, 12, 35, 36]. Due to the study area's ERT incorporated topography data, the finite-element technique with 4 nodes and L2-norm was used for the least-squares inversion. This approach expedited the inversion process and, also, minimized the difference between the measured and calculated apparent resistivities of the inverted models. A damping factor of 0.05, with a minimum value of 0.01, was employed to improve the results of the calculated apparent resistivities and inversion model resistivity sections. The root-mean-square error (RMSE) of the inverse resistivity model converged below 10% for a maximum of 7 iterations.

Moreover, the IPI2win software [37] was used to invert the VES field datasets to generate the resulting model resistivity curves. The model resistivity curve comprises the thickness, depth, and resistivity values of the delineated subsurface layers. High anomalous peaks in a curve compared to the surrounding stations, owing to poor electrode grounding, circuit relay, or current transmission, were corrected via data reduction, remodeling, and re-iteration. Following these corrections, the iteration of such VES field data was repeated. The RMSE of the iteration convergence limit was also less than 10% for all generated VES curves. The generated VES results were used to compute the geohydraulic characteristics of aquifer zones in the study area. Other software, such as Oasis Montaj^{TM} and Geosoft Surfer^{TM}, was used to produce two-and three-dimensional (2-D and 3-D) maps for this study.

3.3. Estimation of Geohydraulic Parameters and Regression Analysis

The hydraulic conductivity (K) and transmissivity (T) of the aquifers, expressed in m/day and m^2/day were, respectively, computed using equations (1) and (2), as presented by [38]. The equations were adopted because the water-bearing units in the study area are within the weathered and fractured hard rock sections sandwiched by resistive layers. Transmissivity gives the areal extent of pore-water flow per day in the saturated aquifer units. The estimated values for K and T were converted from m/sec and m^2/sec to m/day and m^2/day, respectively. In addition to these parameters, the permeability (Ψ) of each aquifer unit was computed using equation (3). The overburden's longitudinal conductance (S) at each VES station point was also estimated using equation (4), as [39] suggested. The hydraulic resistance (K_R), expressed in years, was estimated to ascertain the aquifer vulnerability index (AVI) rating of the aquifer unit in the studied site using equation (5) given by [40]. The logarithm of the hydraulic resistance (log K_R) was also estimated to measure the AVI of the aquifer protective capacity (APC) of the overburden unit to the vertical flow of fluid.

$$K = 8 \times 10^{-6} e^{-0.0013\rho_0} \tag{1}$$

$$T = Kh \tag{2}$$

$$\Psi = Kv_d/\partial_w g \tag{3}$$

$$S = \Sigma_{i=1}^{n} h_i/\rho_i = h_1/\rho_1 + h_2/\rho_2 + \cdots h_n/\rho_n \tag{4}$$

$$K_R = \Sigma_{i=1}^{n} h_i/K_i = h_1/K_1 + h_2/K_2 + \cdots h_n/K_n, \tag{5}$$

where ρ_0 is the resistivity ($\Omega \cdot m$) of the aquifer, σ, S, and h are the conductivity, longitudinal conductance (mho), and the thickness (m) of the aquifer, respectively. v_d, ∂_w, and g are the

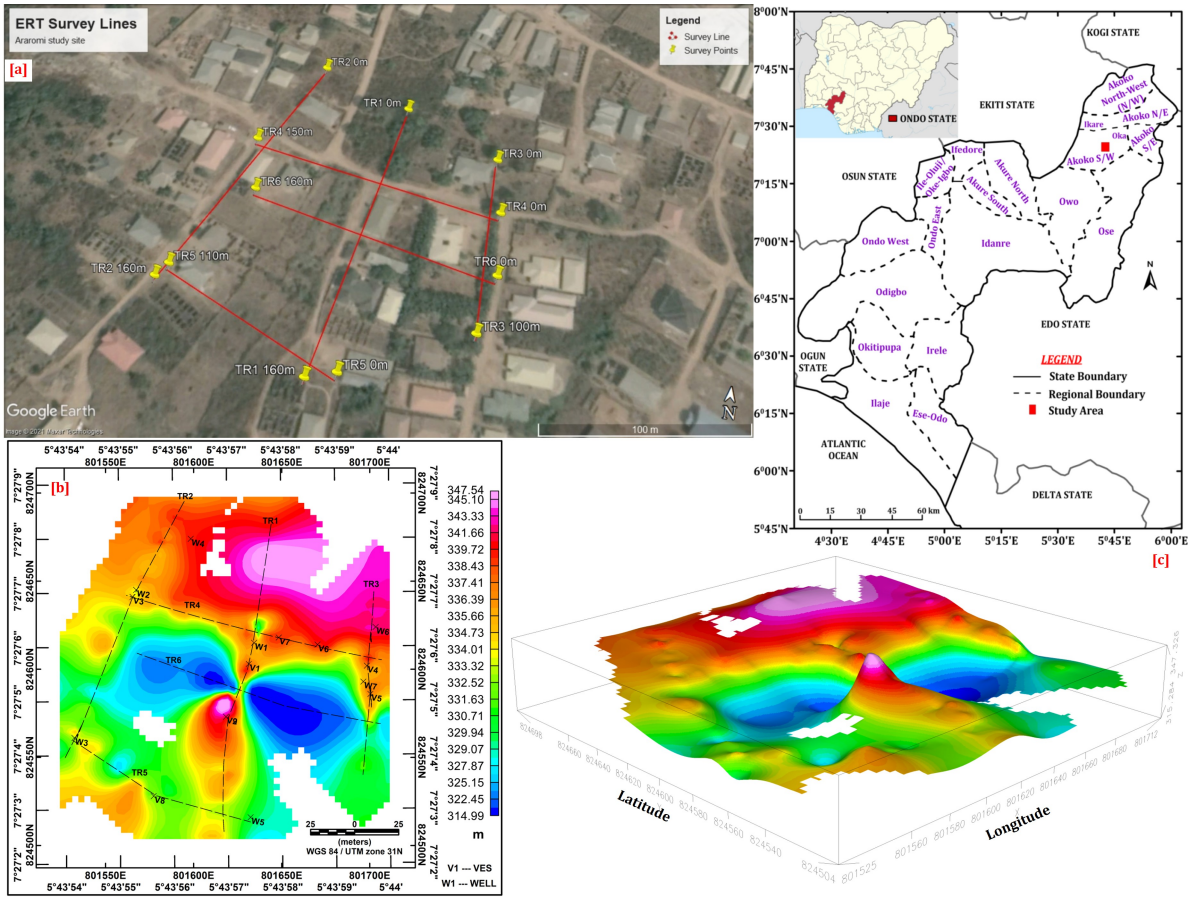

Figure 2: (a) Aerial map showing the traverses and (b) elevation map showing all the VES station points and existing hand-dug wells in the study area. (c) 3-D topographic image of the study area. Inset: Location map of Ondo State showing the study area and surrounding towns.

dynamic water viscosity adopted as 0.0014 kg/m/s according to [41], the density of water (1000 kg/m^3), and the acceleration due to gravity, respectively. ρ_i and h_i are the resistivity and thickness of the i^{th} layer, respectively.

To further substantiate the analyses of the geohydraulic parameters for the Araromi area of Akungba-Akoko, regression analysis was performed using hydraulic conductivity (K) as the independent variable to develop empirical relationships with transmissivity (T), permeability (Ψ), transverse resistance (T_R), longitudinal conductance (S), and hydraulic resistance (K_R), as well as aquifer resistivity (ρ_0). The geostatistical analysis illuminates the relationships between the predicted parameters (i.e., dependent variables) and the independent variables. It also highlights the contribution of each independent variable to posing a vulnerability risk to the aquifers.

4. Results

4.1. Subsurface Lithological and Structural Characterization

The measured resistivity values for the surveyed traverses are presented as composite image and model resistivity sections, depicting the variabilities of the near-surface lithologic units in the study area. A typical example of the composite image derived for the measured and calculated pseudosections, and the inverted model resistivity section for Traverse 1 is shown in Figure 3. Four distinct subsurface layers characterized the study area: topsoil, weathered layer, partially weathered/fractured bedrock, and fresh gneissic bedrock, with resistivities ranging from <10 to >1000 $\Omega \cdot m$, <100 to <1000 $\Omega \cdot m$, 10 to <1000 $\Omega \cdot m$, and >1000 $\Omega \cdot m$, respectively (Figure 3). These given ranges of resistivity values also characterize the delineated layers beneath Traverses 2-6.

In Figure 4, the deep-weathered and fractured zones have varying resistivity signatures due to water saturating fills and their geometries. Stations 30-55 m of Traverse 1 are marked by the deep-weathered trough, while thin-to-large weathered/fractured apertures are delineated beneath stations 15-18 m, 65-70 m, 77 m, and 85-115 m. These zones have been enhanced by five penetrative fractures, represented as F1 to F5 (Figure 4). The water-rock interactions within F4 and F5 created a huge partially weathered bedrock slab between them. The reasonably deep-weathered zone stretching from 140 m to the end of the model is characterized by highly conductive subsurface materials. The subsurface layers beneath Traverse 1 were affirmed by the results of VES 1 and VES 2 at the survey

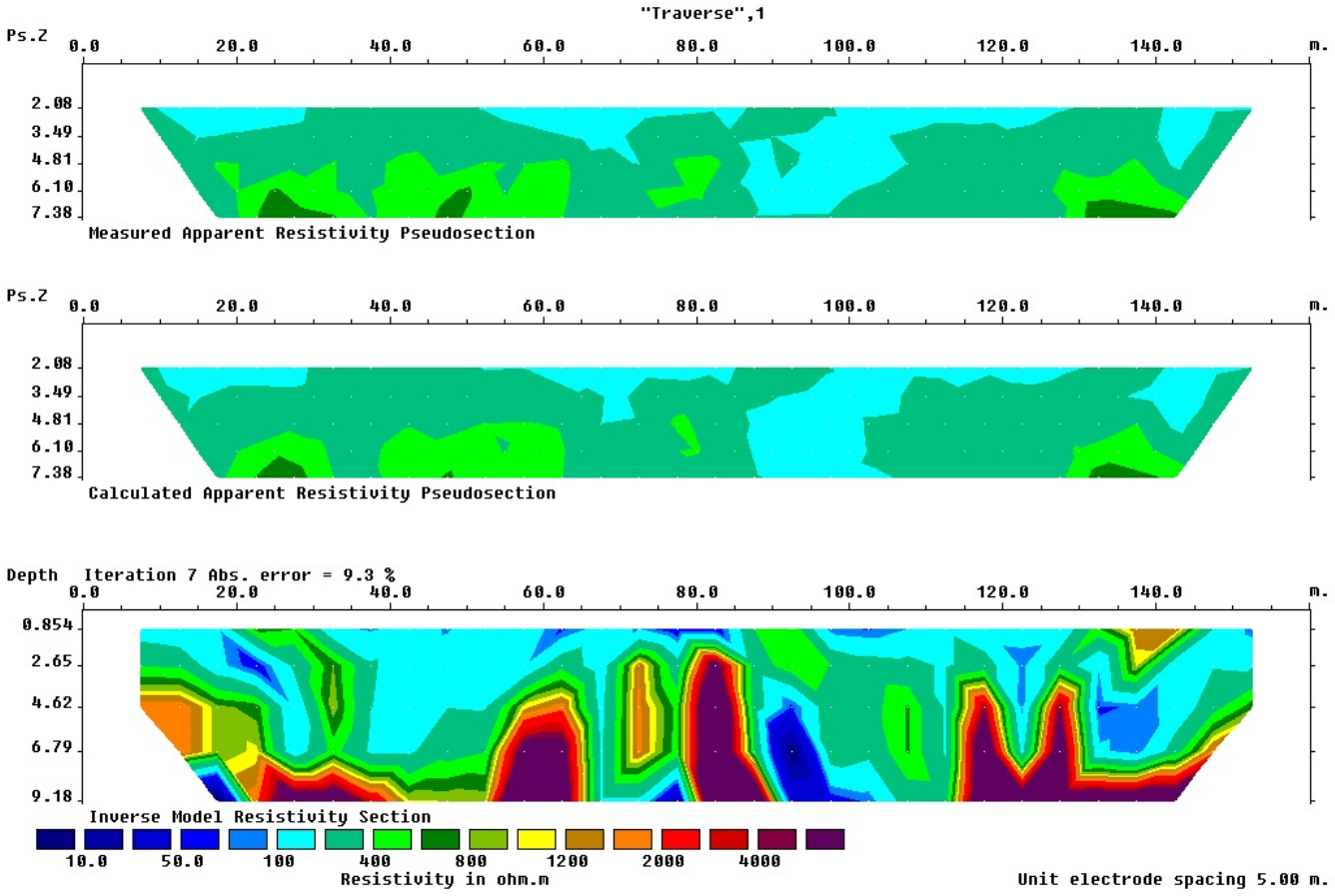

Figure 3: Composite model of the 2-D ERT inversion beneath Traverse 1.

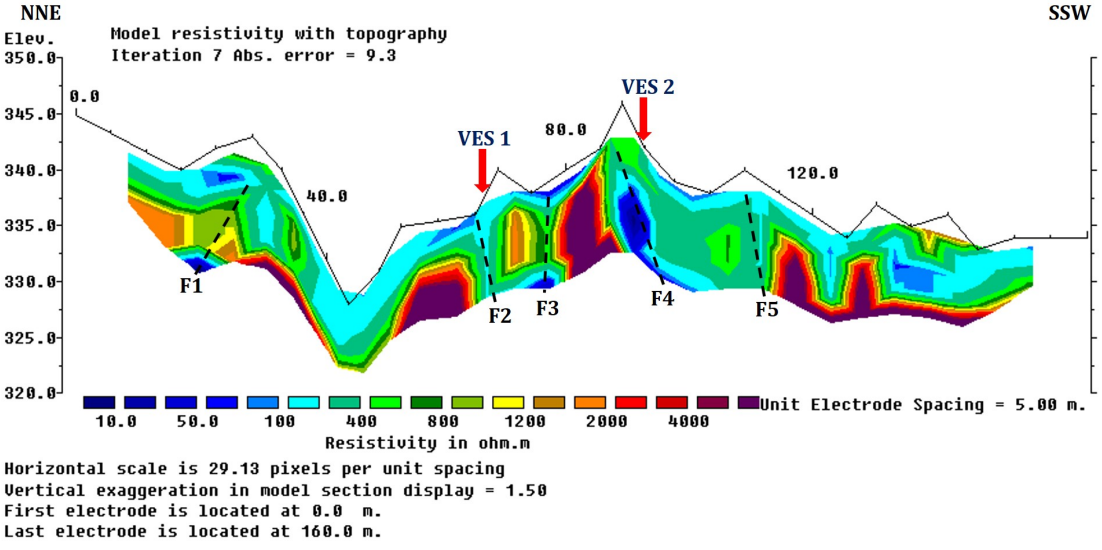

Figure 4: Inverted model resistivity sections beneath Traverse 1 in the study area. The broken dashed lines indicate bedrock fractures.

stations 67.5 m and 95 m. Table 1 presents the results of the VES measurements, including the curve types, thicknesses, depths, and descriptions of the delineated subsurface layers. VES points 1 and 2 are typical KQ and HA curves, respectively (Table 1). A typical example of each generated curve type is shown in Figure 5. Beneath VES points 1 and 2, the topsoil has a thickness of about 1.51 m, and the deep-weathered/fractured zones extend to a depth of about 55 m. The varying degrees of weathered and fractured lithologic sections are clear evidence of intense deformation. This event has contributed significantly

to the groundwater conduits and distributions in the study area.

The resistivity model of Traverse 2 (Figure 6) on the western section with the same parallel profile length as Traverse 1 depicts a low resistive section between surveyed stations 30 m and 40 m, indicating a fractured zone (F6). Also, F7 occurs at surveyed station 55 m within two-segmented highly resistive bedrock. The observed lower resistivity at F7 might be due to the weathered clay-rich residual soil at a depth of <4 m. Fracture (F8) was delineated between station points of 80 m and 130 m. An A-type curve defines the lithologic section beneath VES 3 at station 60 m (Table 1). VES 3 results correlate well with the resistivity model (Figure 6) based on the thicknesses of the delineated layers and the depth to fresh bedrock. The topsoil is about 1.27 m thick, and the weathered profile extends to a depth of 5.67 m (Table 1).

The observed resistivity signatures beneath Traverse 3 (Figure 7) delineate the high resistive zones between geoelectric station points of 20 m and 55 m. These zones correlate with the delineated partially weathered and resistive bedrock segments outcropping at the near-surface from stations 45-48 m, with resistivity values >1000 $\Omega \cdot m$. In addition, low-resistive geoelectric subsurface materials delineated between stations 55-75 m and 80-100 m, with a resistivity of about 200 $\Omega \cdot m$, are identified as water-saturated bedrock zones. These sections act as parts of the groundwater storage features for the study area. Apart from the delineated features, two penetrative fractures (F9 and F10) were imaged between the station positions of 15 m and 25 m, and 50 m and 60 m, respectively. The curve models of VES 4 and VES 5 curve models for geoelectric stations at 45 m and 58 m reveal that the topsoil and the weathered layer beneath Traverse 3 extend to depths of about 3.50 m and 10.30 m at the respective VES points (Table 1). This affirms that the delineated deep-weathered/fractured zones between 80 m and 100 m are deeper than their depths in Figure 7.

The ERT models of Traverses 4, 5, and 6 provide additional subsurface information on lithologies and structures based on the trends, degree of weathering, fracture densities, geometries of anomalous weak zones, and nature of soil compositions in NW-SE. The resistivity model of Traverse 4 (Figure 8) depicts the true nature of the subsurface geologic architecture at the northern section of the studied sites along the NW-SE directions. Like the other traverses, the delineated low resistivity values beneath Traverse 4 indicate deep-weathered troughs and fractures (F11-F13) from the starting station point, and within the station positions of 40-65 m, and 90-105 m. The VES results establish the depths of the weathered and fractured zones beneath Traverse 4 at VES points 6 and 7 with station positions of 35 m and 60 m, respectively (Table 1). From the results, the topsoil (with a resistivity of about 57.5 $\Omega \cdot m$) is delineated with a relatively thin layer (<1.7 m) at VES 6. The saturated to dry sandy weathered materials (zones with resistivity values between 267.6 and 547 $\Omega \cdot m$) extend to a depth of about 6.60 m (but not more than 5.8 m at VES 7). In addition, a depth of 39 m was mapped at VES 7. This depth may have been due to tectonic deformation, which had stretched the depth of either F12 or F13 to fracture the bedrock at a deeper depth.

Furthermore, the geologic conditions towards the southern section in the same parallel direction as Traverse 4 were clearly depicted in Figure 9 (model resistivity section of Traverse 5). Figure 9 shows the subsurface crustal architecture similar to those identified in Traverse 4, especially between the surveyed stations of 20 m and 40 m and 40 m and 100 m. Traverse 5 is characterized by varying low resistive zones arising from the weathered materials and fractures (F14 and F15). These sections demarcate the rugose fresh bedrock between stations 18 m and 30 m, and 70 m and 95 m, respectively. According to VES 8 at point 55 m along Traverse 5, the topsoil has a thickness of about 1.35 m, while the weathered layer has an approximate depth of about 6.52 m (Table 1). However, the depth of the weathered column extends to a depth above 1 m (Figure 9).

The subsurface disparities and similarities between Traverses 4 and 5 are shown by the resistivity model of Traverse 6 (Figure 10). The model depicts a thick overburden subsurface geoelectric profile with probably a high water saturation level. The edges of the bedrock are only seen in a few sections. The topsoil is thicker, extending to a depth of about 3.8 m along this particular geoelectric profile. Six penetrative fractures (F16 to F21) were delineated in Figure 10. The model shows that the near-surface geologic features with deep-weathered sections have high groundwater storage and circulation potential, especially the central depression with F18 and F19. The perfect correlation of the ERT model and VES results proves the accuracy of the methodologies adopted for generating study area's georesistivity results.

5. Discussion

5.1. Near-Surface Architecture of the Study Area

The results of the geoelectric resistivity models for the study area depict four distinct subsurface layers: humus-rich loamy to clayey topsoil, clayey-to-sandy weathered layer, partially weathered/fractured bedrock, and fresh bedrock, with varied resistivities of <10 to >1000 $\Omega \cdot m$, <100 to <1000 $\Omega \cdot m$, 10 to <1000 $\Omega \cdot m$, and >1000 $\Omega \cdot m$, respectively. The varying resistivity values of all the models (Figures 4, 6,7 8, 9, 10) and Table 1 reveal the variability of the weathered materials and water/sand-filled zones. Consequently, the thickness of the topsoil across the study area ranges between 1.16 m and 3.8 m. The delineated partially weathered/fractured zones extend to depths >39 m at VES 7 and >52 m at VES points 1 and 2 (Table 1).

Based on the georesistivity results, the low resistive sections across the area, especially one-third of the Traverse 3 (to-

Table 1: Summary of the generated curve types in relation to the interpreted VES survey station points.

Traverse	VES point	Station (m)	Curve type	Resistivity values ($\Omega \cdot m$)	Thickness, h (m)	Depth, H (m)	Geoelectric interpretation
1	VES1	67.5	KQ	19.4	1.16	1.16	Topsoil (clay rich)
				7847	7.45	8.61	Fresh gneissic bedrock slab
				415	43.6	52.2	Deep weathered trough/fractured
				143	—-		bedrock (water-saturated column)
	VES2	95	HA	110	1.51	1.51	Topsoil
				29.2	3.13	4.64	Water-saturated weathered trough
				699	50.1	54.8	Fractured bedrock slab
				912	—-		Partially weathered trough.
2	VES3	60	A	106	1.27	1.27	Topsoil
				415	4.4	5.67	Sandy weathered trough
				2736	—-		Fresh gneissic bedrock
3	VES4	45	A	158	3.5	3.5	Topsoil
				1218	12.7	16.2	Gradually increasing resistive
				5207	—-		fresh bedrock slab
	VES5	58	A	137	2.59	2.59	Topsoil
				521	7.71	10.3	Sandy weathered trough
				1288	—-		Fresh bedrock slab
4	VES6	35	A	57.5	1.68	1.68	Topsoil
				546	4.92	6.6	Sandy weathered trough
				7451	—-		Fresh bedrock slab
	VES7	60	AK	53.42	1.3	1.3	Topsoil
				267.6	4.5	5.8	Saturated sandy weathered trough
				2476	33.15	38.95	Fresh bedrock slab
				838.1	—-		Fractured bedrock column
5	VES8	55	H	567	1.35	1.35	Topsoil
				138	5.17	6.52	Sandy clay weathered trough
				3872	—-		Fresh bedrock slab

wards the south), indicate the deep-weathered and fracture (F1-F21) zones within the near-surface crustal architecture of the study area. Considering the ERT model of Traverse 6 (Figure 10), the central part of the area is characterized by the highest number of fractures (F16 to F21). In addition, the delineated rugose bedrock surfaces and varying weathered/fractured apertures suggest intense bedrock deformation attributable to the widespread intense metamorphism in the area [3, 42]. Interestingly, the progressive weathering of the subsurface lithologies also enhanced the fractured zones, resulting in open-to-surface fractures. The water-rock interaction enhances the conductivity of near-surface weathered materials, especially in areas with weak zones [5, 10]. Else, the resistive outcrops would have significantly reduced the groundwater potential of the study area. Hence, the groundwater potential of the study area is attributed to the identified subsurface structural features, aiding the conduit and storage of seepages and groundwater flow. On the other hand, the poorly weathered gneissic bedrock across the study area resulted in the development of clayey aquitards and seasonal aquifers with low groundwater yield in hand-dug wells/boreholes [3, 7].

5.2. *Geohydraulic and Geostatistical Evaluation: Insights into Groundwater Yield of the Aquifer Units*

The estimated geohydraulic parameters provide clues on the geohydrodynamics, groundwater yield, and contaminants' vulnerability of the delineated tropically weathered and fractured aquifer units. In addition to the aquifer's resistivity and thickness, the hydraulic conductivity (K) and transmissivity (T) are significant geohydraulic parameters for evaluating the groundwater potential of weathered/fractured bedrock aquifers. The identified weathered and fractured aquifer zones

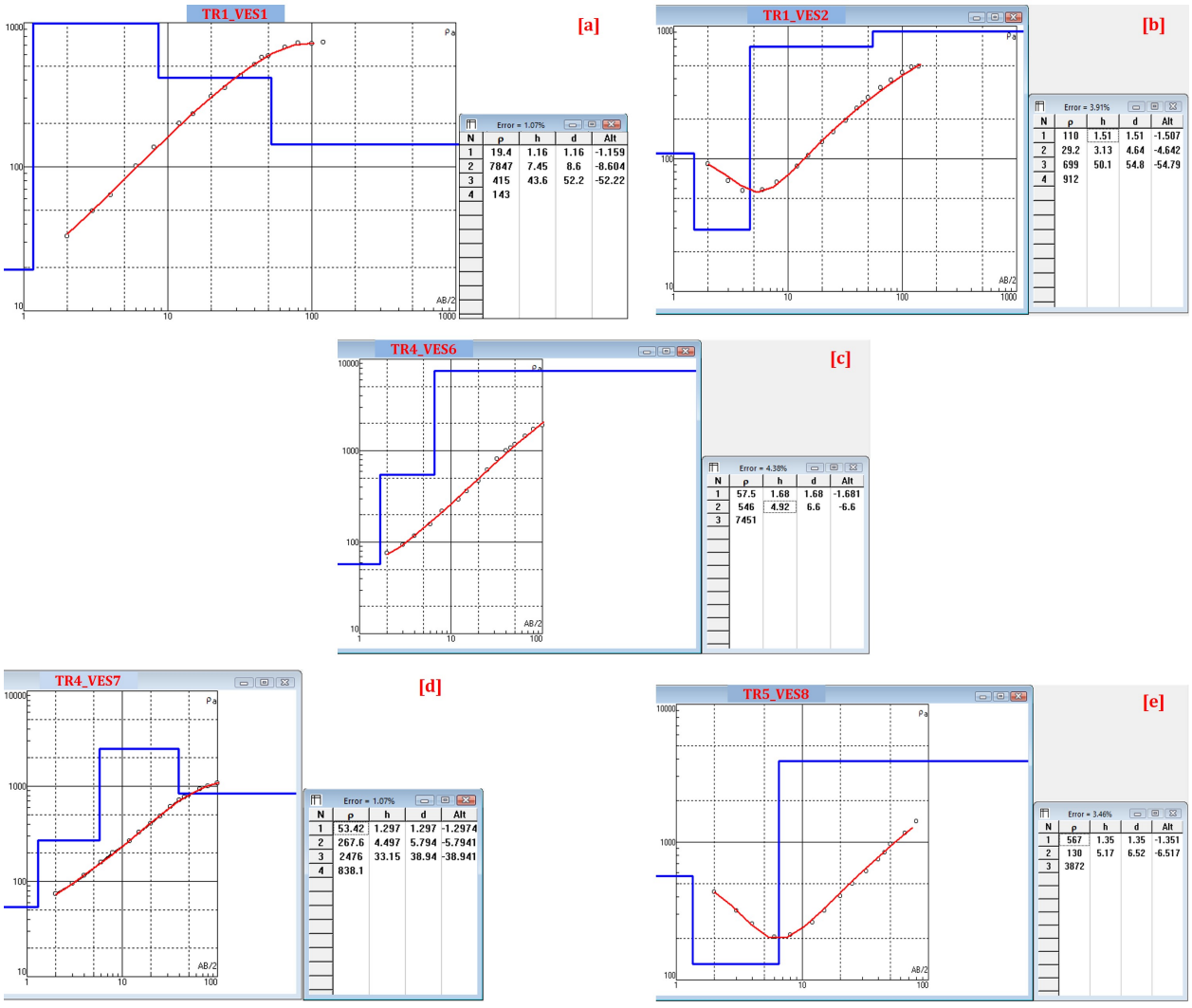

Figure 5: Typical iterated VES curve types generated for the study area: (a) KQ type (VES1), (b) HA type (VES2), (c) A type (VES6), (d) AK type (VES7), and (e) H type (VES8)

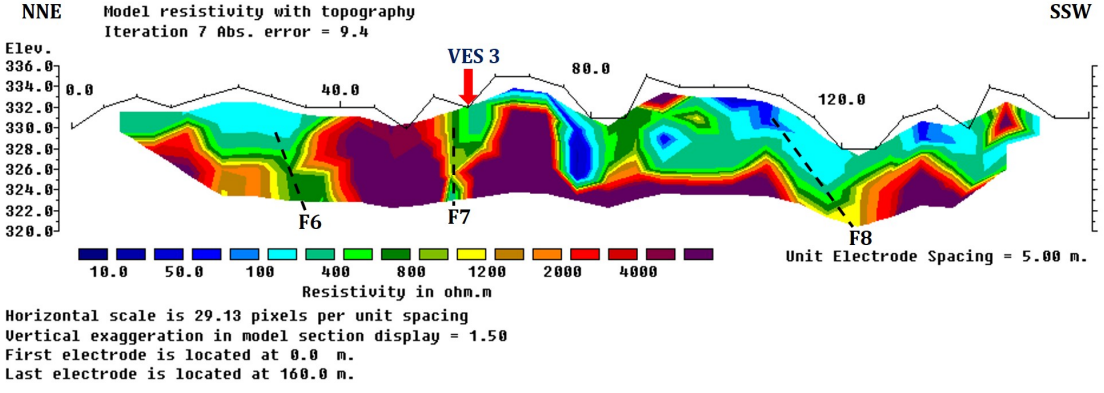

Figure 6: Georesistivity inverted model of Traverse 2.

in the study area were characterized by aquifer resistivity (ρ_0) and thickness (h) values ranging from 138-838.10 $\Omega \cdot m$ and 3.5-50.1 m, respectively (Table 2). The estimated K and T values for the aquifer units in the study area range from 0.23-0.56 m/day and 1.67-17.57 m^2/day, respectively (Table 2). The values of T>7 m^2/day were estimated for VES points 1, 2, and 7. The rest of the VES points recorded values far below this estimated value. This variation may have been due to the

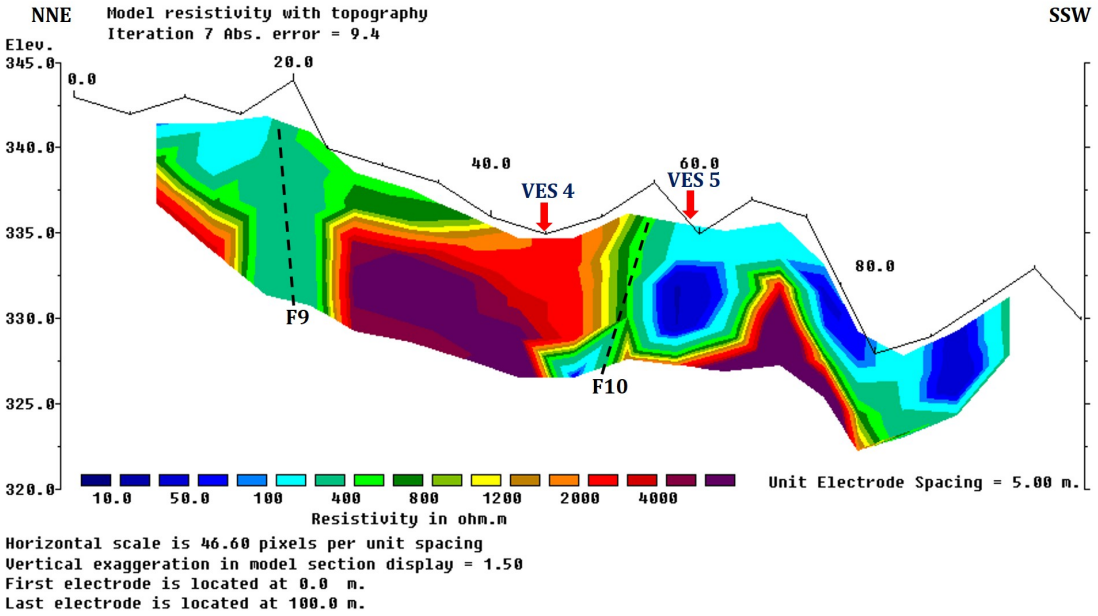

Figure 7: Georesistivity inverted model of Traverse 3.

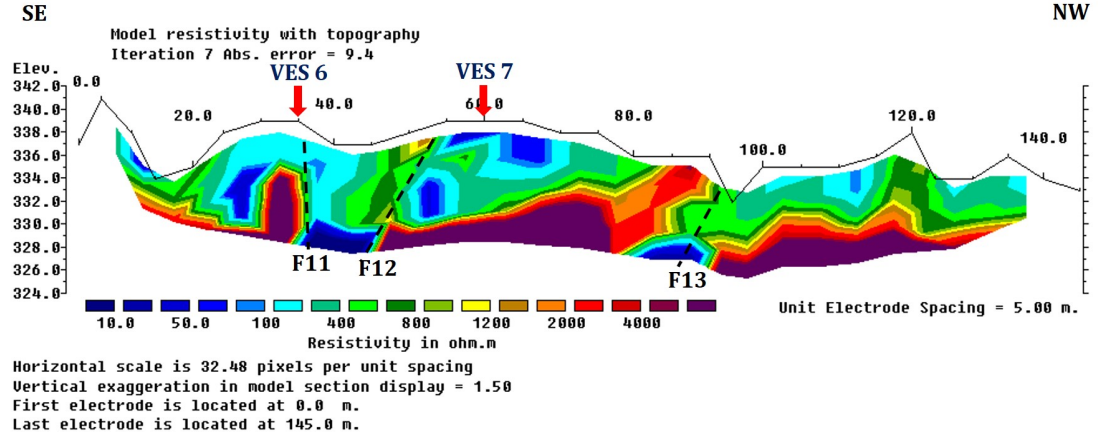

Figure 8: Georesistivity inverted model of Traverse 4.

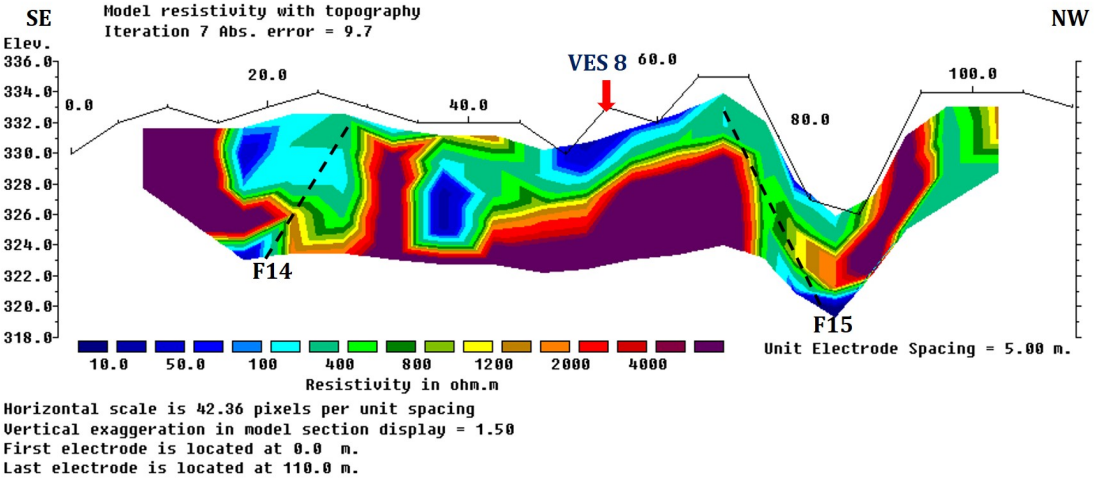

Figure 9: Georesistivity inverted model of Traverse 5.

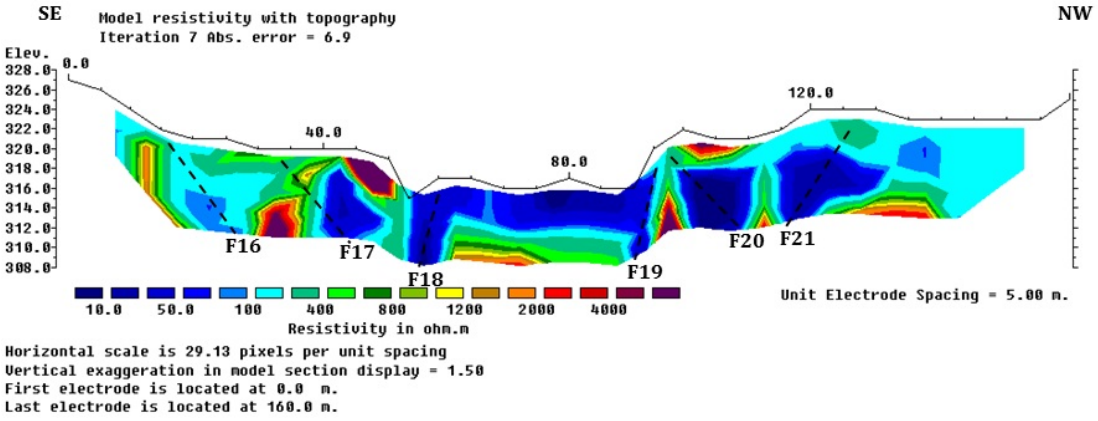

Figure 10: Georesistivity inverted model of Traverse 6.

thicknesses and soil compositions of the weathered/fractured aquifer units, which are responsible for the rate of water-rock interaction from water flows [5, 14]. T and K are directly proportional; hence, this should have increased relationships for both parameters. However, the derived regression result between K and T shows that T decreases for some station points. This variation suggests that the aquifer's thickness is a key factor for T to vary proportionally to K. The estimated permeability (Ψ) values for the aquifer units yielded generally low values ranging from 0.033-0.082 μm^2, indicating the presence of consolidated or weathered clayey materials. The aquifers delineated with high T have lower Ψ values, except VES 1, probably due to decreasing fluid transmissibility in the aquifer units [43].

The regression results (Table 3) provide additional clues on the contribution of each independent variable (ρ_0, T, and Ψ) to the dependent variable (K) for aquifer units in the study area. This analysis is highly important for determining the variability of K with the other estimated geohydraulic parameters because they are all K-dependent. Also, K plays a significant role in evaluating groundwater potential and vulnerability. In Table 3, The K model yielded very strong positive correlation coefficient (R) values with 0.989 and 0.999 for ρ_0 and Ψ, respectively. However, T yielded a very weak positive correlation coefficient value of 0.375. The derived statistical results indicate that ρ_0 and Ψ, with their coefficient of determination (R^2) percentages of 97.8% and 99.9%, and large F-stat values of 271.71 and 5489.03, respectively, are significant in determining K.

High R^2 value for Ψ with K also suggests a significant contribution of both parameters to water-rock interactions [44, 45, 46]. However, the percentage contribution of T to K stands at 14% (Table 3). The low percentage contribution of T with a very low F-stat value of 0.979 indicates a reduction in water transmissivity rate in the aquifers. This could be attributed to the high resistivity values of some aquifers and the occlusion of the weathered/fractured zones by clayey materials. The ρ_0, T, and Ψ decline with K at the values of 0.001, 0.007, and 0.004, respectively. The above-evaluated parameters have low coefficient standard errors, suggesting a very low statistical variation with well-fitted variables in the regression models. The T-stat values with corresponding p-values were used to determine the accuracy and robustness of the analysis. The dependent variables (ρ_0 and Ψ) yielded a p-value ≤ 0.05, except for T. Hence, the result significantly validates the accuracy of the regression analysis. The 95% lower and upper confidence limits ranging from about -0.001 to 0.0001, -0.026 to 0.011, and 6.824-7.291 for ρ_0, T, and Ψ (Table 3) are values to account for the unknown K values for aquifers in the study area [44, 45, 46]. The empirical relationships between K and the parameters ρ_0, T, and Ψ, as given in equations (7)-(10), respectively, could determine K for aquifer units in the study area and other terrains with similar geologic characteristics.

$$K = 0.628 - 0.001\rho_0 \quad (6)$$

$$K = 0.439 - 0.007T \quad (7)$$

$$K = 7.058 - 0.004\Psi \quad (8)$$

Based on the regression results (Table 2), K declines with ρ_0, T, and Ψ. This observation may be due to the progressive weathering of the subsurface geology of the area. These results suggest a possibility for an increase in groundwater yield in the future. Nevertheless, the classifications by [47] were used to determine the groundwater yield capacity of the weathered/fractured aquifer units based on the values of T, as presented in Table 4. Consequently, the study area's tropically weathered and fractured aquifer units are classified as low and moderate groundwater yield aquifers. These aquifer types are efficient for private/personal consumption. However, delineated aquifer zones with deep fractures exceeding 39 m (Table 1) can significantly enhance the groundwater potential of the study area if properly developed. The results further indicate that aquifer transmissibility depends on the physical characteristics of the subsurface geologic units. Therefore, intended hand-dug wells and boreholes are proposed to adequately take advantage of the deep-weathered and fractured zones, with average depths of about 11 m and >39 m,

Table 2: Estimated values for the geohydraulic and vulnerability parameters of the aquifer units in the study area.

VES point	ρ_0 ($\Omega \cdot m$)	h (m)	K (m/day)	T (m^2/day)	$\Psi(\mu m^2)$	S (mho)	K_R (year)	log K_R (year)
1	415	43.6	0.4	17.57	0.058	0.166	108.19	2.03
2	699	50.1	0.28	13.96	0.04	0.193	179.84	2.25
3	415	4.4	0.4	1.77	0.058	0.023	10.92	1.04
4	158	3.5	0.56	1.97	0.08	0.033	6.22	0.79
5	521	7.71	0.35	2.71	0.05	0.034	21.96	1.34
6	547	4.92	0.34	1.67	0.048	0.038	14.49	1.16
7	838.1	34	0.23	7.91	0.033	0.055	146.24	2.17
8	138	5.17	0.58	2.99	0.082	0.04	8.95	0.95
Range	138-838.1	3.50-50.10	0.23-0.56	1.67-17.57	0.033-0.082	0.023-0.193	6.22-179.84	0.79-2.25

Table 3: Regression analysis of the hydraulic conductivity against other estimated aquifer parameters in the study area.

Regression Statistics for K (m/day) Model	ρ_0 ($\Omega \cdot m$)	T (m^2/day)	Ψ (μm^2)	S (mho)	K_R
Multiple R	**0.989**	0.375	**0.999**	0.339	**0.763**
R square (R^2)	**0.9780**	0.140	**0.999**	0.115	0.583
Adjusted R^2	0.9754	-0.003	0.999	-0.032	0.513
Standard error	0.196	1.238	0.004	1.256	0.863
Observations	8				

K model	Coefficient	Constant	Standard error of the coefficient	T Stat	F Stat	p-value	95% Confidence limits of the coefficient	
							Lower	Upper
$\rho_0(\Omega \cdot m)$	-0.001	0.628	0.016	39.531	271.71	<0.0001	-0.001	<0.0001
T (m^2/day)	-0.007	0.439	0.007	6.813	0.979	0.361	-0.026	0.011
Ψ (μm^2)	-0.004	7.058	0.006	-0.647	5489.03	<0.0001	6.824	7.291
S (mho)	-0.627	0.438	0.710	-0.8885	0.782	0.411	-2.364	1.109
log K_R	-1.60	0.627	0.055	7.247	8.375	0.028	-0.295	-0.025

K implies geohydraulic conductivity, which is the dependent variable.

respectively. The proposed zones will significantly increase groundwater supply and make it more sustainable for the host community, AAUA staff, and current and future students inhabiting the area. However, boreholes should be developed with adequate completion procedures to make groundwater supplies in boreholes sustainable due to the observed T and Ψ results. Hand-dug wells in the area may be impacted by infiltration from runoff because they are somewhat shallow in most sections except for the deep-weathered bedrock sections >11 m.

5.3. Vulnerability Assessment of Weathered/Fractured Aquifer Units

The evaluation of aquifer vulnerability in the study area depends on the estimation of the longitudinal conductance S and hydraulic resistance K_R to classify the aquifer protective capacity (APC) and aquifer vulnerability index (AVI) [40, 48, 49]. The K_R is an essential geological formation factor in determining the resistance of an aquifer to vertical fluids flowing through the protective subsurface lithologies. This parameter depends on K but varies inversely proportional to it. The relationship between the AVI and the logarithm of the hydraulic resistance (log K_R) for all the VES points are shown in Table 5. The values of S for the tropically weathered and fractured gneissic aquifers units in the study area range from 0.0226-0.1926 mhos (see Table 2). The values of K_R, on the other hand, varies between 6.22 and 179.84, while the log K_R ranges from 0.79 to 2.25 years (Table 2). The regression of S and K yielded a weak positive correlation value (0.339), with a significant percentage contribution of about 11.5% and an adjusted coefficient of -0.032 based on the results of the R^2 and adjusted R^2, respectively (Table 3). The log K_R yielded a high positive correlation of about 0.763 with K. This parameter contributed about 58.3% to the evaluated K model. The weak positive correlation between K and S suggests that both parameters are independent of one another, just as explained above. K is empirically related to S and log K_R based on equations (9) and (10), and could predict the values of K for the aquifer units in the study area.

$$K = 0.438 - 6.27S \tag{9}$$

$$K = 0.627 - 1.6(\log K_R) \tag{10}$$

Following the reports of [39], the aquifer zones at VES points 1 and 3-8 are characterized by poor APC, while VES 2 has a weak APC (Table 5). On the other hand, the AVI ratings of aquifer units in the study area are characterized by extremely high AVI (VES points 4 and 8), high AVI (VES points

Table 4: Classifications of the groundwater yield potential in relation to the transmissivity of the aquifer unit in the study area (after [47]).

T (m^2/day)	Aquifer potential	Groundwater yield potential	Geoelectric VES station points of the study area
>1000	Very high	Very high water withdrawal of great regional importance	
100-1000	High	Withdrawal of lesser regional importance	
10-100	Moderate	Withdrawal of local water supply for a small community	1 & 2
1-10	Low	Smaller water withdrawal for private consumption	3, 4, 5, 6, 7, & 8
0.1-1	Very low	Withdrawal of local water supply with limited consumption	
<0.1	Negligible	Impermeable sources for local water supply are difficult	

3, 5, and 6), and moderate AVI (VES points 1, 2, and 7), as presented in Table 6. These results classifications were based on the range of $\log K_R$ values, as suggested by [40]. Hence, these results suggest that the Araromi area of Akungba-Akoko is characterized by poor to weak APC, with extremely high to moderate AVI due to the thin overburden. Based on the APC and AVI results, intended hand-dug wells and boreholes in the study area will require adequate protection against infiltrating contaminants to provide sustainable potable groundwater supplies for the inhabitants of the area. The study's findings are consistent with the hydrodynamics and groundwater vulnerability of Etioro-Akoko, a nearby town in the southern part, as reported by [7, 49].

Table 5: Comparison of standard values for the longitudinal conductance and the protective capacity rating for the study area.

Longitudinal conductance, S (mho)	Aquifer protective capacity (APC) rating	Simplified APC ratings of the VES points in the study area based on estimated S values
[39, 48]		
>10	Excellent	
5-10	Very good	
0.7-4.9	Good	
0.2-0.69	Moderate	
0.1-0.19	Weak	2
<0.1	Poor	1 & 3-8

Table 6: Comparison of the standard values for $\log C$ in relation to AVI ratings for the study area (after [40]) .

$\log C$ (years)	Aquifer vulnerability index (AVI)	Classified AVI of the VES points determined based on the $\log C$ for the study area
>4	Extremely low vulnerability	
3-4	Low vulnerability	
2-3	Moderate vulnerability	1,2, & 7
1-2	High vulnerability	3,5, & 6
<1	Extremely high vulnerability	4 & 8

6. Conclusion

The geohydraulic characteristics and contaminants' vulnerability of tropically weathered and fractured gneissic aquifers in the Araromi area of Akungba-Akoko, southwestern Nigeria, have been assessed using a combination of ERT, VES, and regression analysis. In most sections, the topsoil is generally thin (<1.7 m), but the thickness values extend to about 2.5-3.5 m at VES points 4 and 5 along Traverse 3. This study shows that the Araromi area of Akungba-Akoko (the study area) and Etioro-Akoko generally have thin overburden of <4 m with almost similar subsurface geologic characteristics. However, the tropically deep-weathered/fractured bedrock sections extend to depths above 39 m. The regression results indicate that the ρ_0, T, and Ψ, contributed significantly, about 97.8%, 14%, and 99.9%, respectively, to the estimated K parameter for aquifers in the study area. Based on the delineated subsurface lithologic units and geologic structures at varying depths and the geohydraulic characteristics (K, T, and Ψ), the aquifer units in the study area are characterized by low to moderate groundwater yield potential. However, the fractured aquifer zones extending to depths above 52 m can produce adequate groundwater yield. The estimated S values (0.0226-0.1926 mho) for APC ratings in the study are are low. Thus, the APC ratings of the area are rated poor to weak, with extremely high to moderate AVI. As a result, effective construction designs for intended wells/boreholes are critical for adequate protection against infiltrating contaminants in the study area and its surroundings with similar geohydraulic characteristics and vulnerability ratings. This study has provided significant insights into assessing sustainable potable

groundwater development in crystalline basement geologic environments using integrated multi-geophysical resistivity and regression analytical approaches.

Acknowledgements

I thank the Department of Earth Sciences, Adekunle Ajasin University, for providing the field equipment used for this study. Ayanfe Moses Asulewon (formerly of the Department of Earth Sciences, Adekunle Ajasin University) is acknowledged for his assistance during field data acquisition. I also thank the Geophysics Unit, School of Physics, Universiti Sains Malaysia, for providing a conducive research environment. The two anonymous reviewers are greatly appreciated for their impactful comments and suggestions to enrich the scientific quality of this work.

References

[1] M. Offodile, *Ground Water Study and Development in Nigeria*, Mecon Geology and Engineering Service Limited, Jos, Nigeria, (2014).

[2] W.J. Cosgrove & D.P. Loucks, "Water management: current and future challenges and research directions", Water Resources Research **51** (2015) 4823.

[3] A.S. Akingboye, A.A. Bery, J.S. Kayode, A.M. Asulewon, R. Bello, & O.E. Agbasi, "Near-Surface Crustal Architecture and Geohydrodynamics of the Crystalline Basement Terrain of Araromi, Akungba-Akoko, SW Nigeria, Derived from Multi-Geophysical Methods", Natural Resources Research **31** (2022) 215. https://doi.org/10.1007/s11053-021-10000-z.

[4] N.J. George, J.C. Ibuot, D.N. & Obiora, "Geoelectrohydraulic parameters of shallow sandy aquifer in Itu, Akwa Ibom State (Nigeria) using geoelectric and hydrogeological measurements", Journal of African Earth Sciences **110** (2015) 52. https://doi.org/10.1016/j.jafrearsci.2015.06.006.

[5] I. Stober, & K. Bucher, "Hydraulic conductivity of fractured upper crust: insights from hydraulic tests in boreholes and fluid-rock interaction in crystalline basement rocks", Geofluids **15** (2015) 161. https://doi.org/10.1111/gfl.12104.

[6] N.J. George, A.E. Akpan, & F.S. Akpan, "Assessment of spatial distrilbution of porosity and aquifer geohydraulic parameters in parts of the Tertiary - Quaternary hydrogeoresource of south-eastern Nigeria", NRIAG Journal of Astronomy and Geophysics **6** (2017) 422. https://doi.org/10.1016/j.nrjag.2017.09.001.

[7] A.S. Akingboye, & I.B. Osazuwa, "Subsurface geological, hydrogeophysical and engineering characterisation of Etioro-Akoko, southwestern Nigeria, using electrical resistivity tomography", NRIAG Journal of Astronomy and Geophysics **10** (2021) 43. https://doi.org/10.1080/20909977.2020.1868659.

[8] D.N. Obiora, J.C. Ibout, & N.J. George, "Geophysical assessment of potential hydrological units in hydrologically challenged geomaterials of Makurdi, Benue State, Nigeria", International Journal of Physical Sciences **10** (2015) 479. https://doi.org/10.5897/IJPS2015.4386.

[9] W.O. Raji, & K.A. Abdulkadir, "Evaluation of groundwater potential of bedrock aquifers in Geological Sheet 223 Ilorin, Nigeria, using geoelectric sounding", Applied Water Science **10** (2020) 220. https://doi.org/10.1007/s13201-020-01303-2.

[10] M. Hasan, Y. Shang, G. Akhter, & M. Khan, "Geophysical Investigation of Fresh-Saline Water Interface: A Case Study from South Punjab, Pakistan", Groundwater **55** (2017) 841. https://doi.org/10.1111/gwat.12527.

[11] A.S. Akingboye, & A.A. Bery, "Performance evaluation of copper and stainless-steel electrodes in electrical tomographic imaging", Journal of Physical Science **32** (2021) 13. https://doi.org/10.21315/jps2021.32.3.2.

[12] A.S. Akingboye, & A.A. Bery, "Evaluation of lithostratigraphic units and groundwater potential using the resolution capacities of two different electrical tomographic electrodes at dual-spacing", Contributions to Geophysics and Geodesy **51** (2021) 295. https://doi.org/10.31577/congeo.2021.51.4.1.

[13] M. Hasan, Y. Shang, W. Jin, & G. Akhter, "Assessment of Aquifer Vulnerability Using Integrated Geophysical Approach in Weathered Terrains of South China, Open Geosciences **11** (2019) 1129. https://doi.org/10.1515/geo-2019-0087.

[14] M. Hasan, Y. Shang, G. Akhter, & W. Jin, "Delineation of contaminated aquifers using integrated geophysical methods in Northeast Punjab, Pakistan", Environmental Monitoring and Assessment **192** (2020) 12. https://doi.org/10.1007/s10661-019-7941-y.

[15] D.N. Obiora, U.D. Alhassan, J.C. Ibuot, & F.N. Okeke, "Geoelectric Evaluation of Aquifer Potential and Vulnerability of Northern Paiko, Niger State, Nigeria", Water Environment Research **88** (2016) 644. https://doi.org/10.2175/106143016X14609975746569.

[16] A.M. Ekanem, "Georesistivity modelling and appraisal of soil water retention capacity in Akwa Ibom State University main campus and its environs, Southern Nigeria", Modeling Earth Systems and Environment **6** (2020) 2597. https://doi.org/10.1007/s40808-020-00850-6.

[17] A.S. Akingboye, I.B. Osazuwa, & M.Z. Mohammed, "Electrical resistivity tomography for geoengineering investigation of subsurface defects: A case study of Etioro-Akoko highway, Ondo State, Southwestern Nigeria", Studia Quaternaria **37** (2020) 101. https://doi.org/10.24425/sq.2020.133754.

[18] M.Z. Mohammed, T.H.T. Ogunribido, & A.T. Funmilayo, "Electrical resistivity sounding for subsurface delineation and evaluation of groundwater potential of Araromi Akungba-Akoko Ondo State southwestern Nigeria", Journal of Environment and Earth Science **2** (2012) 29. www.iiste.org.

[19] M.B. Aminu, "Electrical Resistivity Imaging of a Thin Clayey Aquitard Developed on Basement Rocks in Parts of Adekunle Ajasin University Campus, Akungba-Akoko, South-western Nigeria", Environmental Research, Engineering and Management **71** (2015) 47. https://doi.org/10.5755/j01.erem.71.1.9016.

[20] M.A. Rahaman, *Review of the Basement Geology of southwestern Nigeria*, in: C.A. Kogbe (Ed.), Geology of Nigeria, Elizabeth Publisher. Co., Lagos, (1976).

[21] M.A. Rahaman, *Recent advances in the study of the Basement Complex of Nigeria*, in: P.O. Oluyide, W.C. Mbonu, A.E.O. Ogezi, I.G. Egbuniwe, A.C. Ajibade, A.C. Umeji (Eds.), Precambrian Geology of Nigeria, Geological Survey of Nigeria, Kaduna, (1988).

[22] A. Kröner, B.N. Ekwueme, & R.T. Pidgeon, "The Oldest Rocks in West Africa: SHRIMP Zircon Age for Early Archean Migmatitic Orthogneiss at Kaduna, Northern Nigeria", The Journal of Geology **109** (2001) 399.

[23] N.G. Obaje, "Geology and Mineral Resources of Nigeria", Springer Berlin Heidelberg, Berlin, Heidelberg, (2009). https://doi.org/10.1007/978-3-540-92685-6.

[24] B.J. Fagbohun, A.A. Omitogun, O.A. Bamisaiye, & F.J. Ayoola, "Gold potential of the Pan African Trans-Sahara belt and prospect for further exploration", Ore Geology Reviews **116** (2020) 103260. https://doi.org/10.1016/j.oregeorev.2019.103260.

[25] A.C. Ogunyele, S.O. Obaje, A.S. Akingboye, A.O. Adeola, A.O. Babalola, & A.T. Olufunmilayo, "Petrography and geochemistry of Neoproterozoic charnockite-granite association and metasedimentary rocks around Okpella, southwestern Nigeria", Arabian Journal of Geosciences **13** (2020) 780. https://doi.org/10.1007/s12517-020-05785-x.

[26] K.M. Goodenough, P.A.J. Lusty, N.M.W. Roberts, R.M. Key, & A. Garba, "Post-collisional Pan-African granitoids and rare metal pegmatites in western Nigeria: Age, petrogenesis, and the 'pegmatite' conundrum," Lithos **200-201** (2014) 22. https://doi.org/10.1016/j.lithos.2014.04.006.

[27] A.C. Ogunyele, O.A. Oluwajana, I.Q. Ehinola, B.E. Ameh, & T.A. Salaudeen, "Petrochemistry and petrogenesis of the Precambrian Basement Complex rocks around Akungba-Akoko, southwestern Nigeria", Materials and Geoenvironment **66** (2020) 173. https://doi.org/10.2478/rmzmag-2019-0036.

[28] A.S. Akingboye, O. Ademila, C.C. Okpoli, A. V. Oyeshomo, R.O. Ijaleye, A.R. Faruwa, A.O. Adeola, & A.A. Bery, "Radiogeochemistry, uranium migration, and radiogenic heat of the granite gneisses in parts of the southwestern Basement Complex of Nigeria", Journal of African Earth Sciences **188** (2022) 104469. https://doi.org/10.1016/j.jafrearsci.2022.104469.

[29] A.S. Akingboye, A.C. Ogunyele, A.T. Jimoh, O.B. Adaramoye, A.O. Adeola, & T. Ajayi, "Radioactivity, radiogenic heat production and environmental radiation risk of the Basement Complex rocks of

Akungba-Akoko, southwestern Nigeria: insights from in situ gamma-ray spectrometry", Environmental Earth Sciences **80** (2021) 228. https://doi.org/10.1007/s12665-021-09516-7.

[30] S.M.A. Adelana, P.I. Olasehinde, R.B. Bale, P. Vrbka, A.E. Edet, & I.B. Goni, *An overview of the geology and hydrogeology of Nigeria*, in: Applied Groundwater Studies in Africa, (2008). https://doi.org/10.1201/9780203889497-13.

[31] M. Woakes, M.A. Rahaman, & A.C. Ajibade, "Some metallogenetic features of the Nigerian basement", Journal of African Earth Sciences **6** (1987) 655. https://doi.org/10.1016/0899-5362(87)90004-2.

[32] M.H. Loke, *Rapid 2D resistivity and IP inversion using the least-square method - Geoelectrical Imaging 2-D and 3D*, (2004).

[33] A.S. Akingboye & A.C. Ogunyele, "Insight into seismic refraction and electrical resistivity tomography techniques in subsurface investigations", Rudarsko Geolosko Naftni Zbornik **34** (2019) 93. https://doi.org/10.17794/rgn.2019.1.9.

[34] M.H. Loke & R.D. Barker, "Practical techniques for 3D resistivity surveys and data inversion 1", Geophysical Prospecting **44** (1996) 499. https://doi.org/10.1111/j.1365-2478.1996.tb00162.x.

[35] C. DeGroot-Hedlin & S. Constable, "Occam's inversion to generate smooth, two-dimensional models from magnetotelluric data", Geophysics **55** (1990) 1613. https://doi.org/10.1190/1.1442813.

[36] M.H. Loke, J.E. Chambers, D.F. Rucker, O. Kuras, & P.B. Wilkinson, "Recent developments in the direct-current geoelectrical imaging method", Journal of Applied Geophysics **95** (2013) 135. https://doi.org/10.1016/j.jappgeo.2013.02.017.

[37] A. Kurniawan, *Basic IP2 Win Tutorial: Basic Principles in Using IP2 Win Software*, (2009).

[38] K.P. Singh, "Nonlinear estimation of aquifer parameters from surficial measurements", Hydrology and Earth System Sciences **2** (2005) 917. https://doi.org/10.5194/hessd-2-917-2005.

[39] M. Oladapo, M. Mohammed, O. Adeoye, & B. Adetola, "Geoelectrical investigation of the Ondo State Housing Corporation Estate Ijapo Akure, southwestern Nigeria", Journal of Mining and Geology **40** (2004) 41. https://doi.org/10.4314/jmg.v40i1.18807.

[40] D. Van Stempvoort, L. Ewert, & L. Wassenaar, Aquifer vulnerability index: A GIS - compatible method for groundwater vulnerability mapping, Canadian Water Resources Journal **18** (1993) 25. https://doi.org/10.4296/cwrj1801025.

[41] C.W. Fetter, *Applied Hydrogeology*, 4th ed., Waveland Press, Inc., Long Grove, Illinois, (2018). https://www.amazon.com/Applied-Hydrogeology-C-W-Fetter-ebook/dp/B07CM8Y415 (accessed March 20, 2022).

[42] M.A. Rahaman, *Review of the basement geology of SW Nigeria*, in: C.A. Kogbe (Ed.), Geology of Nigeria, Elizabeth Publishing. Co. Nigeria, (1989). http://www.sciepub.com/reference/51950 (accessed March 20, 2022).

[43] N.J. George, J.C. Ibuot, A.M. Ekanem, & A.M. George, "Estimating the indices of inter-transmissibility magnitude of active surficial hydrogeologic units in Itu, Akwa Ibom State, southern Nigeria", Arabian Journal of Geosciences **11** (2018) 134. https://doi.org/10.1007/s12517-018-3475-9.

[44] R.J. Freund, D. Mohr, & W.J. Wilson, *Statistical Methods*, Elsevier, 2010. https://doi.org/10.1016/C2009-0-20216-9.

[45] G. Smith, *Multiple Regression, in: Essential Statistics, Regression, and Econometrics*, Elsevier, (2012). https://doi.org/10.1016/B978-0-12-382221-5.00010-6.

[46] A.S. Akingboye, & A.A. Bery, "Characteristics and rippability conditions of near-surface lithologic units (Penang Island, Malaysia) derived from multimethod geotomographic models and geostatistics", Journal of Applied Geophysics **204** (2022) 104723. https://doi.org/10.1016/j.jappgeo.2022.104723.

[47] J. Krasny, "Classification of Transmissivity Magnitude and Variation", Ground Water **31** (1993) 230. https://doi.org/10.1111/j.1745-6584.1993.tb01815.x.

[48] J.P. Henriet, "Direct applications of the Dar-Zarrouk parameters in groundwater surveys", Geophysical Prospecting **24** (1976) 344. https://doi.org/10.1111/j.1365-2478.1976.tb00931.x.

[49] A.S. Akingboye, A.A. Bery, J.S. Kayode, A.C. Ogunyele, A.O. Adeola, O.O. Omojola & A.S. Adesida, "Groundwater-yielding capacity, water-rock interaction, and vulnerability assessment of typical gneissic hydrogeologic units using geoelectrohydraulic method", Acta Geophysica, (2022). https://doi.org/10.1007/s11600-022-00930-4.